PERGAMON

Vacuum 53 (1999) 113–116

VACUUM
SURFACE ENGINEERING, SURFACE INSTRUMENTATION & VACUUM TECHNOLOGY

Microstructure and mechanical properties of multilayer TiB_2/C and co-sputtered TiB_2-C coatings for cutting tools

M.A. Baker,* R. Gilmore, C. Lenardi, P.N. Gibson, W. Gissler

European Commission, Institute for Advanced Materials, Joint Research Centre, I-21020 Ispra (Va), Italy

Abstract

The feasibility of reducing the friction coefficient of TiB_2-based coatings by the incorporation of carbon has been investigated for both multilayer and co-sputtered coatings. Characterisation was performed using pin-on-disk tribometry, nanoindentation, glancing angle X-ray diffractometry, X-ray photoelectron and Auger electron spectroscopy. The co-sputtered coatings were found to consist of two phases: a hexagonal TiB_2-type structure into which carbon is incorporated and a diamond-like carbon (DLC) phase. C is preferentially incorporated into the $Ti(B,C)_2$ phase and the lubricating DLC phase only starts to form once saturation is reached. Consequently, a reduction in the friction is only found at total C concentrations higher than 50 at%. For the multilayers, there was an increase in the overall carbon content required to obtain a friction-reducing effect from about 10–50 at% as the TiB_2 sublayer thickness was decreased from 100 to 1 nm. This was attributed to an increase in the relative proportion of carbon bonded with TiB_2 in the interface regions. Coatings with a hardness of about 20–30 GPa and friction coefficients of < 0.2 against a steel ball could be obtained at a suitable composition. © 1999 Elsevier Science Ltd. All rights reserved.

Keywords: Hard coatings; Low friction; TiB_2; Carbon; Multilayers

1. Introduction

There is a strong industrial interest in developing coatings which combine high hardness and low friction, for example, to advance cutting tool technology and permit lubricant-free machining [1]. A previous study has demonstrated the feasibility of producing low-friction coatings by incorporating the lubricant phase (C or MoS_2) within the hard-coating structure [2]. In the case of C-containing coatings, carbon's lubricating efficiency appeared to be adversely affected by its tendency to incorporate into the hard phase, thus restricting the formation of a distinct carbon phase [2,3]. In the present study, we report our findings for multilayer TiB_2/C coatings and make a direct comparison with the co-sputtered TiB_2-C coatings. The coatings have been characterised by, XPS/AES, GAXRD, nanoindentation and pin-on-disk testing.

2. Experimental

Film deposition was performed with a commercially available magnetron sputtering device in which a TiB_2, a graphite and a Ti target were mounted. The base chamber pressure was 1×10^{-6} Pa. Stainless-steel substrates were mechanically polished to an average roughness of less than 100 nm, degreased and ultrasonically cleaned. Prior to deposition, the substrates were RF sputter etched (1 kW) using Ar, at a rate of 0.3 nm s^{-1}, for 10 min followed by deposition of an 15 nm adhesion-promoting Ti interlayer. Gas contamination was of the order of 0.3%. The TiB_2 target was DC sputtered at 300 W and the C target RF sputtered at 1 kW with a substrate temperature of approximately 150°C.

To obtain co-sputtered coatings of varying composition, the substrates were placed in different positions along the centreline between the TiB_2 and C targets. Multilayer coatings were prepared using the same deposition parameters and the substrates alternately placed under the TiB_2 and C targets using a programmable rotating platter. Three series of multilayers were

* Corresponding author. Tel.: 39 0332 785277; fax: 39 0332 785036; e-mail: mark.baker@jrc.it

0042-207X/99/$ – see front matter © 1999 Elsevier Science Ltd. All rights reserved.
PII: S0042-207X(98)00404-7

prepared with sputtering times programmed to theoretically give 100, 10 and 1 nm TiB_2 sublayers. The first sublayer deposited was always TiB_2 and the final sublayer C. Coating thickness was about 3 μm.

XPS spectra were taken using an unmonochromated Al Kα source (360 W) on a Cameca Nanoscan 50 at an energy resolution of 0.5 eV. Ar^+ etching to remove the surface oxide and depth profile was performed by rastering a 3 keV, 0.2 μA ion beam. Quantification of the spectra was performed using relative sensitivity factors determined from TiB_2, TiC and TiO_2 standards. The B and C 1s peaks were curve fitted using a mixed Gaussian/Lorentzian function after a Shirley background subtraction. AES profiles were recorded on a PHI 560 spectrometer using a 3 keV, 1 μA electron beam and 4 keV Ar^+ ion beam.

Glancing Angle X-ray Diffraction (GAXRD) was performed on an in-house constructed instrument using an unmonochromated copper source at an incident angle of 0.5°. The beam is collimated by a high precision variable slit positioned between the source the sample and a Soller slit collimator is mounted between the sample and detector for angular resolution. A solid state detector is used to isolate the Cu Kα doublet and reduce the background noise level to a minimum.

Hardness was determined from the loading and unloading curves recorded by an ultra-low load depth-sensing nanoindenter (Nanoindenter II, from Nano Instruments Inc.). Elastic contributions were determined from the unloading curve. The measurements were calibrated with a Si (1 1 1) wafer assuming a modulus of 157 GPa, independent of penetration depth. Under these conditions a penetration depth independent hardness of 12 GPa was obtained for the Si wafer.

A pin-on-disk tribometer (CSEM) was used to measure the friction coefficient at room temperature in laboratory air. The counterface material was a 100Cr6, steel ball, 6 mm in diameter, with a hardness of H_V 800 and roughness R_a of 0.003 μm. A normal load of 5 N and a sliding speed was 0.1 m/s was used at a track radius of 3.5 mm over a 1000 m distance.

3. Results

The atomic percent of C is used as a reference to classify the various coatings. In the case of co-sputtered samples, this is derived from the stoichiometries experimentally determined by XPS analysis. In the case of multilayer coatings, C content is calculated from TiB_2 and C sublayer thickness (based on deposition rate calibration) and assumes a density of 3.9×10^{22} molecules/cm^3 for the TiB_2 sublayer and a density of 17.6×10^{22} atoms/cm^3 for the C sublayer, assuming also a 2:1 B:Ti ratio. This has been verified for a TiB_2:C 1:0.75 nm multilayer coating. Assuming a homogeneous elemental distribution, which for this very thin multilayer coating, is not an unreasonable approximation, XPS analysis gave a C content of 53 at%, the same as the calculated value (see Table 2). XPS determined coating compositions as a function of substrate position are given in Table 1 and calculated compositions as a function of sublayer thickness in Table 2.

Table 1
Composition of multiphase samples

Distance of substrate from middle of TiB_2 target (mm)	Stoichiometry	C content (at%)
57	$TiB_{1.8}C_{0.8}$	22
84	$TiB_{1.7}C_{1.2}$	31
111	$TiB_{1.3}C_{2.2}$	48
138 (centre point between targets)	$TiB_{1.1}C_{3.4}$	61
165	$TiB_{1.4}C_{8.4}$	78
192	$TiB_{1.4}C_{23}$	91

Table 2
Composition of multilayer samples

TiB_2 sublayer thickness (nm)	C sublayer thickness (nm)	Calculated C content (at%)
100	50	43
	20	23
	10	13
	5	7
	2	3
	1	1.5
10	10	60
	5	43
	2	23
	1.5	18
	1.0	13
1	0.75	53
	0.50	43

A detailed interpretation of the GAXRD and XPS spectra for the co-sputtered samples has been given previously [3]. Here, only the salient points will be described. The XRD spectra showed the presence of only one Ti-based phase, exhibiting a hexagonal TiB_2-type structure. No TiC was observed. With increasing C concentration, the (0 0 1) and (0 0 2) peaks shifted to lower diffraction angles and the (1 0 0) peak to higher angles. At C contents greater than 60 at%, the TiB_2-type phase entered the nanocrystalline to amorphous transition region, and at 90 at% C, the sample was amorphous. The XPS C 1s peak showed the presence of two strong components at 284.5 and 282.9 eV (also found in the multilayer samples, see Fig. 1a). The 284.5 eV component corresponds to predominantly sp^2 hybridised C–C bonding (graphite standard 284.45 eV), i.e. diamond-like carbon (DLC). The 282.9 eV component has a binding energy indicative of carbon bonded to a more

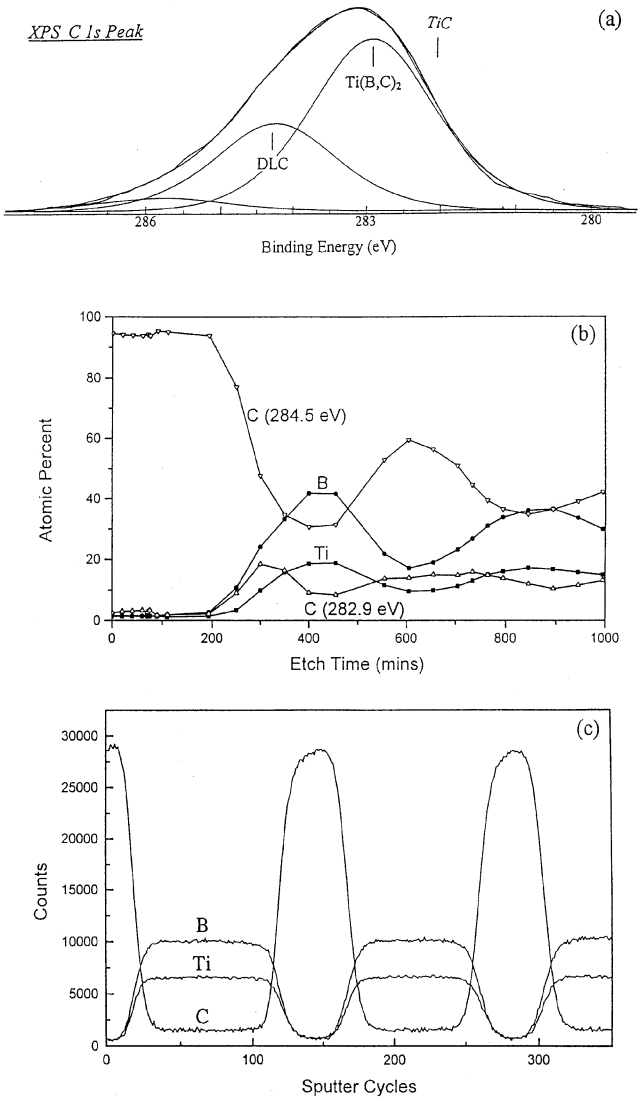

Fig. 1. Results for the multilayer samples (a) TiB_2 : C 1 : 0.75 nm, XPS C 1s peak (b) TiB_2 : C 10 : 10 nm, XPS depth profile (c) TiB_2 : C 100 : 50 nm, Auger depth profile.

electropositive element, but the peak position is significantly different to TiC (281.8 eV). A binding energy value of 282.9 eV may be explained by carbon in an environment where it bonds both to titanium and boron. The B 1s peak exhibited one strong component at 188.0 eV (TiB_2 standard 187.75 eV), which shifts to higher binding energies with increasing C content. The C and B 1s peak positions indicate a partial substitution of B by C and possibly additional incorporation of interstitial carbon in the TiB_2 structure. The C fraction of the $Ti(B,C)_2$ phase increases with total C content.

In Fig. 1, the results from three multilayer samples are presented. Fig. 1a shows the C 1s peak from the TiB_2 : C 1 : 0.75 nm multilayer. Clearly, the photoelectron escape depth extends over a number of layers, making a profile redundant. As for the multiphase samples, the C peak is composed of two components, corresponding to the $Ti(B,C)_2$ and DLC phases. Assuming a homogeneous distribution of the elements, the sample was calculated to have a stoichiometry of $TiB_{1.9}C_{3.3}$ and a carbon content of 53 at% , of which only 18 at% corresponded to the DLC phase. An XPS profile for a TiB_2 : C 10 : 10 nm multilayer is presented in Fig. 1b. Although the profile quality is affected by the sample roughness, it can be seen from the first interface, that the $Ti(B,C)_2$ phase formation is concentrated in the interfacial region. From a single bilayer, which was chosen to be the first TiB_2 layer and second C layer in the profile an average value of 14 at% C was bonded as $Ti(B,C)_2$. As the total C content has been calculated to be 60 at% (Table 2), the DLC content in this sample is estimated at 46 at%. Fig. 1c shows an Auger depth profile of a TiB_2 : C 100 : 50 nm multilayer. The clear distinction of the TiB_2 and C bilayers and the small interfacial volume indicates that the amount of C bonded as $Ti(B,C)_2$ in the sample is negligible and the DLC content can be estimated to be similar to the total C content which has been calculated to be 43 at%.

The hardness and friction coefficient as a function of the C content is presented in Fig. 2a for the multiphase samples and Fig. 2b for the multilayers. The multiphase samples show an S-shaped dependence, with high hardness (45 GPa) and high friction coefficient (0.85) at low

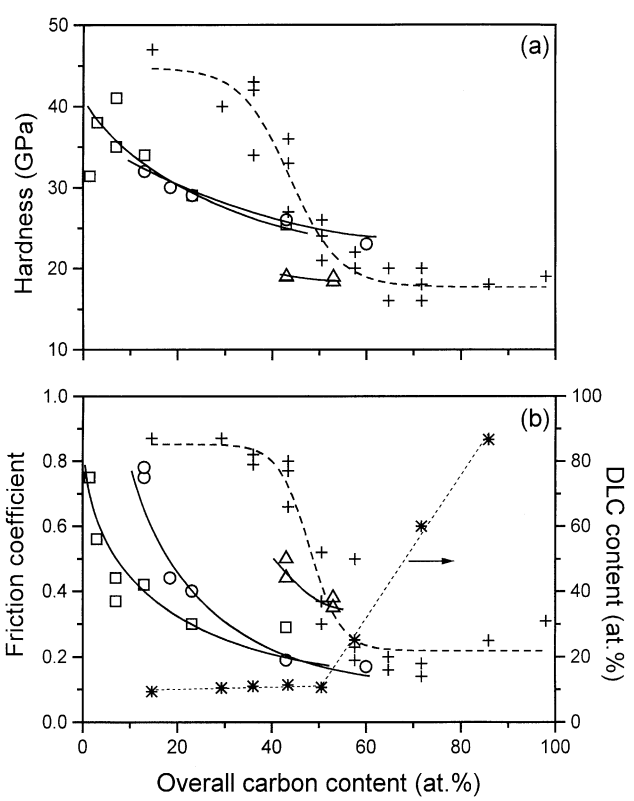

Fig. 2. As a function of C content: (a) Hardness; (b) Friction coefficient and DLC content: multilayer samples: TiB_2 : C 100 nm (□), 10 nm (○), 1 nm (△), multiphase samples TiB_2/C (+); DLC content (∗).

C contents, the transition to lower hardness (20 GPa) and lower friction coefficient (0.2) occurring between 40 and 60 at% C. The multilayer samples show a progressive reduction in hardness (from 40 GPa) and friction coefficient (from 0.8) with increasing C content, due to a continuous decrease of the hard TiB_2 phase content and an increase of the softer lubricating C phase. Increasing the TiB_2 sublayer thickness strongly reduces the amount of C required to obtain low friction.

4. Discussion and conclusions

The GAXRD and XPS results have shown that carbon is being incorporated into the TiB_2 structure. In Fig. 2a, the concentration of C atoms bonded in the DLC phase, determined from the XPS results, is plotted as a function of C content. The concentration of DLC remains below 15 at% until the total C content attains about 50 at%, and then increases sharply. This behaviour occurs due to the strongly differing free energies of formation of the two C containing phases. $Ti(B,C)_2$ is a metastable phase but may be considered to have a ${}^{f}\Delta G^{0}_{298}$ somewhat similar to that of TiB_2 (-317 kJ/mol). DLC will have a ${}^{f}\Delta G^{0}_{298}$ very similar to that of graphite (0 kJ/mol). Consequently, C preferentially bonds as $Ti(B,C)_2$ and DLC forms only when no more C can be accommodated in the $Ti(B,C)_2$ phase.

The trends in the mechanical properties can now be understood. In the multiphase samples, much of the C is being tied up in the $Ti(B,C)_2$ phase and the amount of lubricating DLC phase required to produce low friction needs to be correlated with the DLC content and not the total C content. From Fig. 2a, the content of DLC required to reduce the friction to 0.2 can be estimated to be between 20 and 30 at%. The results from the multilayer samples in Fig. 2b are in agreement with this. The very thin multilayer sample having a DLC content of 18 at%, has a medium friction of about 0.4. The other two multilayer samples, both containing about 45 at% DLC, show friction coefficients values of 0.2–0.3. The best dual property performance was found for the multiphase samples to be obtained for a $TiB_{1.2}C_{3.4}$ sample, giving a hardness of 20 GPa and a friction coefficient of < 0.2 and for the multilayers was a TiB_2 : C 10 : 5 nm, sample $TiB_2C_{2.3}$ (calculated composition) showing a hardness of 27 GPa and a friction coefficient of < 0.2.

Acknowledgements

We would like to acknowledge the invaluable technical assistance of A. Hoffmann, T. Sasaki, L.Mammarella and P. Salvatore.

References

[1] Cselle T, Barimani A. Surf Coat Technol 1995;76–77:712.
[2] Gilmore R, Baker MA, Gibson PN, Gissler W. Surf Coat Technol 1998;105:45.
[3] Baker MA, Gilmore R, Gibson PN, Gissler W. In: Olefjord I, Nyborg L, Briggs D, editors. ECASIA 97. Chichester: Wiley, 1997:1127.